

Comparison of the $\text{Ca}^{2+}/\text{COO}^-$ Complexation Induced Controllable Aggregation of P(VCL-*co*-NaA) Spherical Microgels and Linear Chains

Shufu Peng and Chi Wu*

The Open Laboratory of Bond-selective Chemistry, Department of Chemical Physics, University of Science and Technology of China, Hefei, Anhui, China, and Department of Chemistry, The Chinese University of Hong Kong, Shatin, Hong Kong

Received March 1, 2001; Revised Manuscript Received May 21, 2001

ABSTRACT: The $\text{Ca}^{2+}/\text{COO}^-$ complexation induced aggregation of poly(*N*-vinylcaprolactam-*co*-sodium acrylate) (P(VCL-*co*-NaA)) spherical microgels as well as linear chains under different conditions, such as the Ca^{2+} concentration, the COO^- content, and the aggregation temperature, was studied by a combination of static and dynamic laser light scattering. Using thermally sensitive P(VCL-*co*-NaA) enabled us to vary the chain conformation and the sticking efficiency of two collided spherical microgels or linear chains by temperature, so that the aggregation was controllable and reversible. The time evolution of both the weight-average molar mass (M_w) and the average hydrodynamic radius ($\langle R_h \rangle$) of the aggregates was simultaneously recorded. It showed that for the microgel aggregates M_w could be scaled to $\langle R_h \rangle$ as $M_w \propto \langle R_h \rangle^{d_f}$ and the average scattering intensity $I(q)$ varied with the scattered vector q as $I(q) \propto q^{-d_q}$ with d_f and d_q in the range 1.6–1.9, indicating a diffusion-limited process, while for the chain aggregates, both d_q and d_f decreased from ~ 2.5 to ~ 1.6 as the aggregation temperature increased from 32.5 to 50 °C, revealing, for the first time, that the structure of the resultant aggregates depends on the initial chain conformation. For both spherical microgels and linear chains, the aggregation rate and the aggregate size increased with the Ca^{2+} concentration, but the structures of the resultant aggregates remained.

Introduction

The cation induced aggregation of colloid particles in a dispersion or polyelectrolytes chains in a solution is not only fascinating and interesting in basic research but also important in many applications,¹ such as the production of chemical toners, the treatment of wastewater, and the making of membrane filters. Numerous theoretical^{2–5} and experimental^{6–9} efforts have been devoted to the formation and structure of colloidal aggregates. Two limiting regimes have been identified as the diffusion-limited cluster–cluster aggregation (DLCA) and the reaction-limited cluster–cluster aggregation (RLCA).^{10,11} One of distinctive features between DLCA and RLCA is different fractal dimensions (d_f) of the resultant aggregates,¹² i.e., different scalings between the mass (M) and size (R) of the aggregates, $M \sim R^{d_f}$. To which regime an actual aggregation process falls is essentially governed by the sticking efficiency between two collided particles. In DLCA, every collision leads to an irreversible sticking, and the aggregation rate is limited solely by the time required for two particles to encounter each other by diffusion. The DLCA process leads to the formation of aggregates with an open and less uniform structure and $d_f \sim 1.75–1.80$ for a three-dimensional system. The kinetics of DLCA is characterized by a power law $R \sim t^\alpha$ with $\alpha < 1$, where t is the aggregation time.¹³ On the other hand, the sticking probability in RLCA is so low that a number of collisions can only result in one sticking. The RLCA process often happens in hyperbranching polymerization. Experimental observation¹⁴ and the computer simulations^{15,16} have revealed a higher fractal dimension in the range $\sim 2.0–2.5$; namely, the aggregates have a more uniform structure because when a microgel collides with an aggregate, it can penetrate into the

“fjords” of the aggregate before they stick together.¹⁷ Weitz et al.¹³ suggested that the RLCA process follows an exponential kinetics, i.e., $R \sim e^{At}$, where A is a constant, depending on the dispersion studied. A combination of different scattering techniques provides a possibility to study the formation and structures of colloidal aggregates over a wide size range.^{18–22}

The study has been extended to the complexation of biopolymers because of its implications in ecology, biotechnology, and medicine.^{23,24} In this aspect, the aggregation and complexation of much better defined synthetic polyelectrolytes can be used as a minimal representation of various processes related to biopolymers. The association kinetics and interaction mechanism of synthetic polyelectrolytes have been extensively studied.^{25–27} It was found that the rate constant of the interaction increased sharply with decreasing the polycation ionic strength but was independent of the polyanion chain length.^{28,29} It was suggested that the distribution of ionic groups on the chain backbone had no effect on the complexation.³⁰ Unfortunately, most of the past studies were conducted in a poorly controlled and irreversible fashion. To our knowledge, the influence of initial chain conformation on the formation and structure of the aggregates has not been thoroughly investigated.

In the present study, using thermally sensitive poly(*N*-vinylcaprolactam-*co*-sodium acrylate) (P(VCL-*co*-NaA)), we can use temperature to alter the chain conformation from coil to globule without changing the degree of ionization and the chain length. This is because PVCL is hydrophilic and soluble in water at the room temperature and gradually becomes hydrophobic and insoluble when the temperature increases from ~ 25 to ~ 35 °C.³¹ The copolymerization of a few percent of NaA into PVCL makes the chain more hydrophilic. When the temperature is lower than ~ 30 °C, PVCL is so hydrophilic that the strength of the

* Corresponding author. E-mail chiwu@cuhk.edu.hk.

complexation between Ca^{2+} and COO^- groups is not sufficient to pull different microgels or chains together. As the temperature increases, the balance between hydrophilic solvation and hydrophobic attraction is gradually broken so that the complexation leads to intrachain contraction and interchain aggregation. A comparative study of the complexation induced aggregation of P(VCL-*co*-NaA) spherical microgels and linear chains is conducted by using a combination of static and dynamic laser light scattering (LLS). The influence of temperature, charge density, and cation concentration on the formation and structures of the aggregates was studied.

Experimental Section

Materials. *N*-Vinylcaprolactam monomer (VCL, courtesy of BASF, Germany) was purified by reduced pressure distillation. Sodium acrylate monomer (NaA, from Lancaster) was used without further purification. Potassium persulfate as initiator (KPS, from Aldrich) and *N,N*-methylenebis(acrylamide) as cross-linking agent (MBAA, from Aldrich) were recrystallized three times in methanol. Calcium chloride (anhydrous CaCl_2 , from ACROS) was used without further purification.

Sample Preparation. Spherical poly(*N*-vinylcaprolactam-*co*-sodium acrylate) microgels were prepared by precipitation polymerization. Into a 150 mL three-neck flask equipped with a reflux condenser, a thermometer, and a nitrogen-bubbling tube were added VCL monomer (7.3 mmol), NaA comonomer, MBAA cross-linking agent (0.18 mmol), and deionized water (40 mL). The solution was stirred and bubbled by nitrogen for 1 h to remove oxygen before adding an aqueous solution of KPS (0.05 mmol) to start the polymerization at 60 °C for 24 h. The resultant P(VCL-*co*-NaA) microgels were purified by a successive four cycles of centrifugation (Sigma 2K15 ultracentrifuge, at 15 300 rpm and 40 °C), decantation, and redispersion in deionized water to remove unreacted low molar mass molecules. Three different kinds of microgels were prepared. On average, they contained 1.0, 4.3, and 9.1 mol % acrylic groups, denoted as G-P(VCL-1.0A), G-P(VCL-4.3A), and G-P(VCL-9.1A), respectively, where "G" stands for microgels. The weight-average molar masses of G-P(VCL-1.0A), G-P(VCL-4.3A), and G-P(VCL-9.1A) microgels were 1.33×10^9 , 2.08×10^9 , and 5.41×10^9 g/mol, respectively. The dispersions were diluted to 1.00×10^{-5} g/mL for the LLS study. Linear P(VCL-*co*-NaA) chains containing 4.6 mol % acrylic groups, denoted as L-P(VCL-4.6A), was prepared in a similar way without adding the cross-linking agent (MBAA). The weight-average molar mass of L-P(VCL-4.6A) was 3.04×10^6 g/mol. The concentration of linear chains used in the LLS study was 1.20×10^{-5} g/mL.

Laser Light Scattering. A modified commercial light scattering spectrometer (ALV/SP-125) was used, which was equipped with a multi- τ digital time correlator (ALV-5000) and a solid-state laser (ADLAS DPY 425II, output power \approx 400 mW at $\lambda = 532$ nm). The detail of our laser light scattering spectrometer can be found elsewhere.³² In static LLS, the angular dependence of the absolute excess time-averaged scattered intensity, known as the Rayleigh ratio $R_v(q)$, is related to the weight-average molar mass (M_w), the z -average root-mean-square radius of gyration ($\langle R_g^2 \rangle_z^{1/2}$ or written as $\langle R_g \rangle$) of the scattering objects, and the second virial coefficient (A_2) of the dispersion or solution by

$$\frac{KC}{R_v(q)} \approx \frac{1}{M_w} \left(1 + \frac{1}{3} \langle R_g^2 \rangle_z q^2 \right) + 2A_2 C \quad (1)$$

where $K [= (4\pi^2 n_1^2 / \lambda_0^4 N_A) (dn/dc)^2]$ is a constant and $q [= (4\pi n_1 / \lambda_0) \sin(\theta/2)]$ is the scattering vector with N_A , dn/dc , n_1 , λ_0 , and θ being Avogadro's number, the specific refractive index increment, the refractive index of solvent, the wavelength of the light in a vacuum, and the scattering angle, respectively.

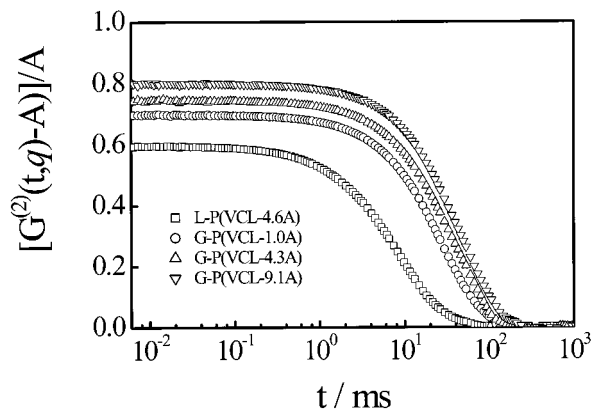


Figure 1. Typical measured intensity–intensity time correlation function of P(VCL-*co*-NaA) spherical microgels and linear chains in water at $\theta = 15^\circ$ and $T = 25^\circ\text{C}$.

By measuring $R_v(q)$ of a very dilute solution at a relatively small angle, we can estimate M_w . For a fractal object made of colloid particles, the scattered intensity $I(q)$ is scaled to q as $I(q) \sim q^{-d_f}$ in the range of $R_{\text{aggregate}} > q^{-1} > R_{\text{particle}}$, where d_f is the fractal dimension; R_{particle} and $R_{\text{aggregate}}$ are the radii of primary particles and the resultant aggregate, respectively.¹⁹ When $q^{-1} < R_{\text{particle}}$, the light probes internal structures of primary particles, and the intensity profile reflects the density distribution inside, while when $q^{-1} > R_{\text{aggregate}}$, the average size of the resultant aggregates and the correlation of the topological length between the aggregates could be determined.

In dynamic LLS, the cumulant or Laplace inversion analysis of the measured intensity–intensity time correlation function $G^{(2)}(q, t)$ in the self-beating mode can lead to an average line width ($\langle \Gamma \rangle$) or a line width distribution ($G(\Gamma)$).^{33,34} For a pure diffusive relaxation, Γ can be related to the translational diffusion coefficient D via $\Gamma = Dq^2$ at $C \rightarrow 0$ and $q \rightarrow 0$ ³⁵ or the hydrodynamic radius (R_h) by the Stokes–Einstein equation, $D = k_B T / (6\pi\eta R_h)$, where k_B , T , and η are the Boltzmann constant, the absolute temperature, and the solvent viscosity, respectively. Therefore, $G(\Gamma)$ can be converted to a hydrodynamic radius distribution $f(R_h)$. All the dynamic LLS measurements were carried out at 15° .

Results and Discussion

Figure 1 shows that a typical plot of the measured intensity–intensity time correlation function for spherical microgels and linear chains in water at $T = 25^\circ\text{C}$. From each correlation function, we were able to calculate an average line width by using the second-order cumulants fitting or the line width distribution (or the hydrodynamic radius distribution) by the CONTIN method. Figure 2 shows typical hydrodynamic radius distributions of spherical microgels and linear chains at 25°C before and after adding Ca^{2+} . It shows that both microgels and linear chains are reasonably narrowly distributed. The relative distribution width ($\mu_2 / \langle \Gamma \rangle^2$) for spherical microgels and linear chains are ~ 0.05 and ~ 0.18 , respectively. The addition of Ca^{2+} led to the shrinking of both spherical microgels and linear chains. However, it should be stated that the addition of Ca^{2+} did not alter the scattering intensity. Therefore, the shrinking of spherical microgels and linear chains can be respectively attributed to the intraparticle and intrachain $\text{Ca}^{2+}/\text{COO}^-$ complexation. For each $f(R_h)$, we were able to calculate one average hydrodynamic radius $\langle R_h \rangle$ by using $\langle R_h \rangle = \int_0^\infty f(R_h) R_h dR_h$. Figure 3 shows that without Ca^{2+} spherical microgels and linear chains gradually shrink as the temperature increases, but no change in molar mass, clearly indicating that there exists no interparticle or interchain aggregation even

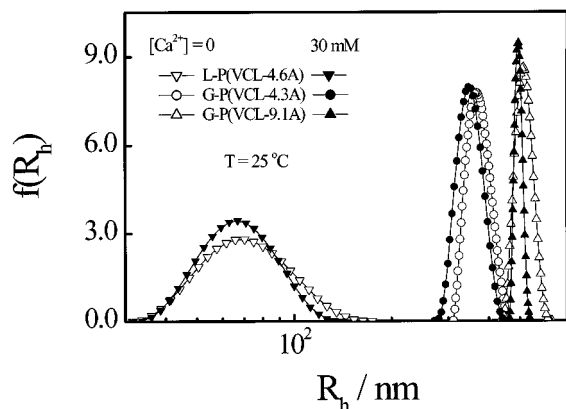


Figure 2. Hydrodynamic radius distributions of P(VCL-co-NaA) spherical microgels and linear chains at $T = 25^\circ\text{C}$ with and without the addition of Ca^{2+} .

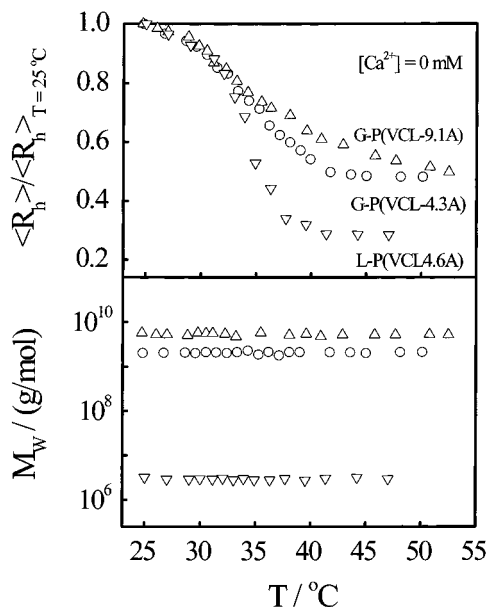


Figure 3. Temperature dependence of average hydrodynamic radius (R_h) of different microgels and linear chains in the absence of Ca^{2+} ions. The inset shows a corresponding temperature dependence of the weight-average molar mass M_w .

at higher temperatures. Relatively, microgels shrink less because they swell less at 25°C due to the cross-linking. However, the situation was completely different after adding Ca^{2+} .

Figure 4 shows that the $\text{Ca}^{2+}/\text{COO}^-$ complexation can induce an interparticle aggregation after the dispersion temperature was suddenly increased from 30 to 32.5°C . As expected, the extent of the aggregation for a given Ca^{2+} concentration increases with the ionic content because each COO^- group acts as a "sticker" in the interparticle or interchain aggregation via the $\text{Ca}^{2+}(\text{COO}^-)_2$ complexation. The aggregation slows down after a few hours and gradually approaches a plateau. It is worth noting that the resultant aggregates were very stable, and no precipitation was observed for a long time. For spherical microgels, $\langle R_h \rangle$ can be scaled to t by $\langle R_h \rangle \propto t^\beta$ with β in the range 0.16–0.20. However, the aggregation of linear chains has a different kinetics; namely, the increase of $\langle R_h \rangle$ can be described by two exponential terms, representing two distinct processes. The initial fast process is related to the aggregation of individual chains and the formation of clusters, while the second slow process mainly involves the cluster-

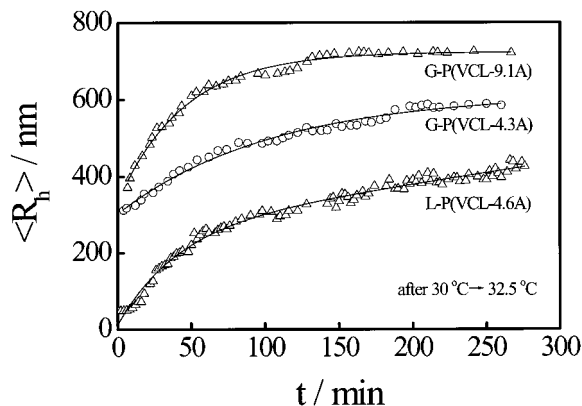


Figure 4. Time dependence of average hydrodynamic radius (R_h) of the aggregates made of different spherical microgels and linear chains, where $[\text{Ca}^{2+}] = 30 \text{ mM}$ and $T = 32.5^\circ\text{C}$.

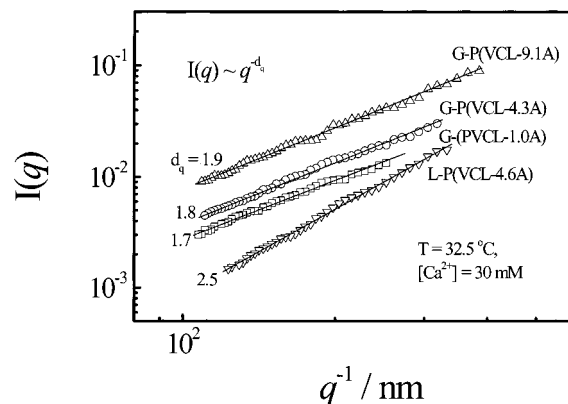


Figure 5. Double-logarithmic plots of scattering intensity $I(q)$ vs scattering vector q for resultant aggregates made of different spherical microgels and linear chains, where $[\text{Ca}^{2+}] = 30 \text{ mM}$ and $T = 32.5^\circ\text{C}$.

cluster aggregation. It should be noted that $\langle R_h \rangle$ is a complicated parameter, and it involves not only the structure but also the hydrodynamic draining. To obtain the fractal dimension from the kinetics, one should measure the time dependence of radius of gyration (R_g). Unfortunately, the aggregation was so fast that we were not able to do it.

Figure 5 shows that the scattering intensity $I(q)$ of the resultant aggregates is dependent on the scattering vector q as $I(q) \propto q^{-d_q}$ with $d_q = 1.7$ – 1.9 for spherical microgels and $d_q = 2.4$ – 2.5 for linear chains, indicating that the aggregation of spherical microgels follows the DLCA process, but the aggregation of linear chains might be described by the RLCA mechanism. For spherical microgels, the slight decrease of d_q as the COO^- content increases indicates that the structure of the aggregates made of microgels with less COO^- groups is relatively more open and less uniform. Note that d_q for linear P(VCL-co-NaA) chains is higher than ~ 2.0 – 2.2 observed in the aggregation/association of other linear chains, such as in the HPAM/ Ca^{2+} system.¹⁴ This is because, in addition to the interpenetration of different chains, the collapse of PVCL at higher temperatures leads to a more uniform structure. The packing of spherical microgels or linear chains in the resultant aggregates can be better viewed in terms of the size dependence of the average chain density (ρ) defined as $M_w / [(4/3)\pi\langle R_h \rangle^3]$.

Figure 6 shows that during the aggregation $\langle \rho \rangle$ decreases as the aggregation proceeds, clearly indicating

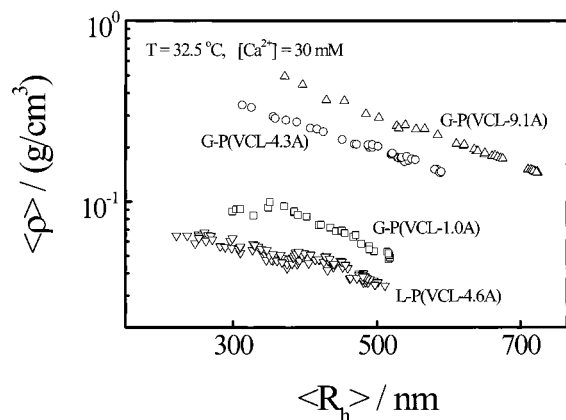


Figure 6. Aggregate size dependence of average chain density $\langle \rho \rangle$ for different spherical microgels and linear chains, where $[\text{Ca}^{2+}] = 30 \text{ mM}$ and $T = 32.5^\circ\text{C}$.

that the aggregates become loose and less uniform. Unfortunately, $\langle \rho \rangle$ and $\langle R_h \rangle$ only spread over a limited range. A combination of Figures 5 and 6 shows that for a given size the aggregates made of microgels have a lower d_q and chain density. It also shows that the aggregates made of linear chains have a much lower chain density but a higher d_q . This is because, in comparison with the microgels, there are no chemical cross-linking among different chains in the aggregates made of linear chains. Therefore, the interchain distance inside is larger so that the chain density is lower. Thermodynamically, there should be an entropy penalty when individual microgels are stick together, but the intertwining and knotting of linear chains could lead to a possible entropy gain. It is expected that the enthalpy change in the formation of each $\text{Ca}^{2+}(\text{COO}^-)_2$

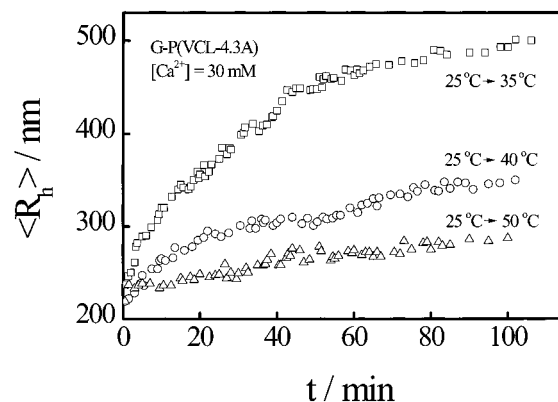


Figure 8. Time dependence of average hydrodynamic radius $\langle R_h \rangle$ of microgel aggregates formed after the dispersion temperatures were suddenly increased to different aggregation temperatures.

complex is a constant. Therefore, the increase of entropy makes a process more favorable. Figure 7 shows a schematic of the $\text{Ca}^{2+}/\text{COO}^-$ complexation induced aggregation of spherical microgels and linear chains at higher temperatures. The difference in the linear chain aggregation at different temperatures is presented and discussed as follows.

Figure 8 shows that for a given Ca^{2+} concentration the growth of $\langle R_h \rangle$ is less pronounced as the aggregation temperature increases. This is different from what we expected. Originally, we thought that PVCL at a higher temperature was more hydrophobic so that the aggregation should be enhanced. However, we forgot that PVCL collapses more at a higher aggregation temperature. After a sudden temperature increase, individual microgels collapse before they have a chance to be stuck

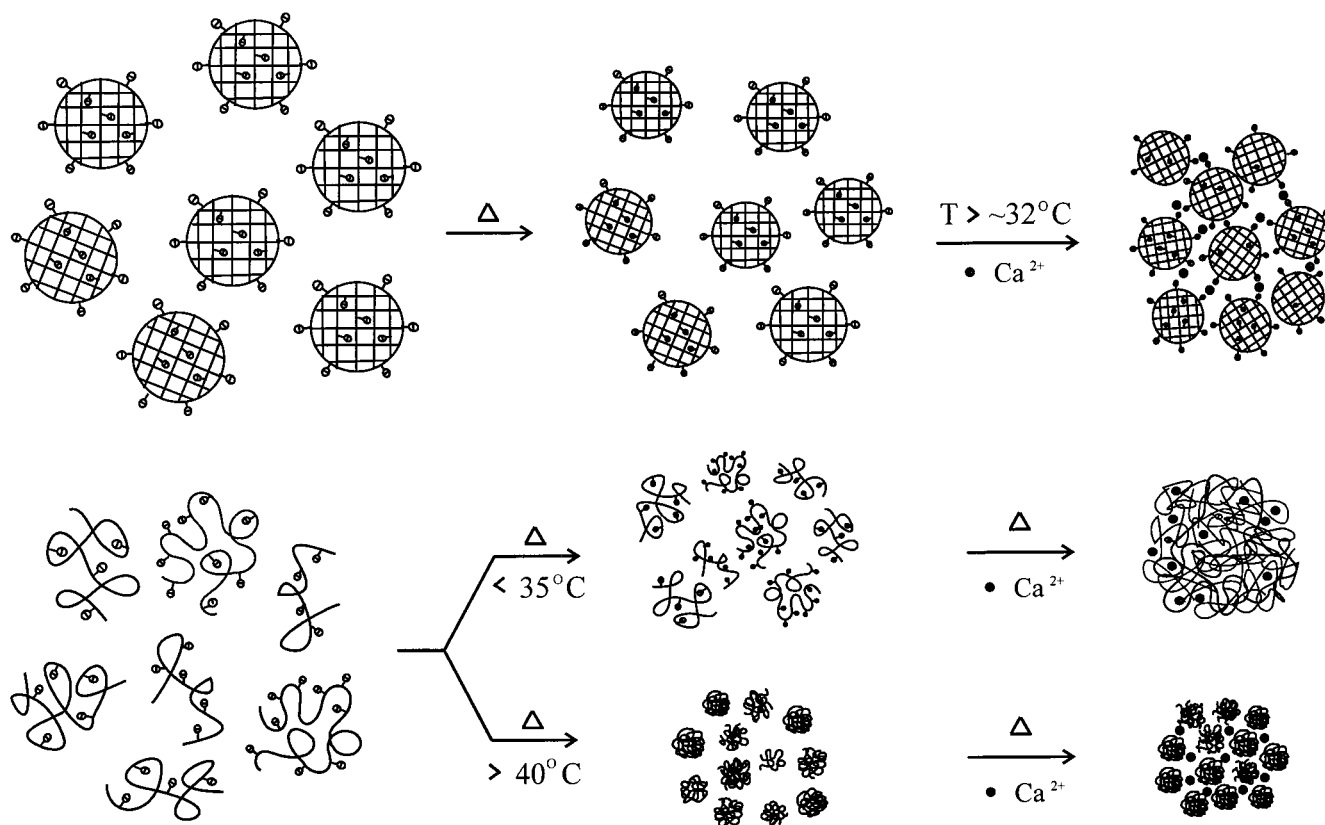


Figure 7. Schematic of $\text{Ca}^{2+}/\text{COO}^-$ complexation induced aggregation of thermally sensitive P(VCL-co-NaA) spherical microgels and linear chains at higher temperatures.

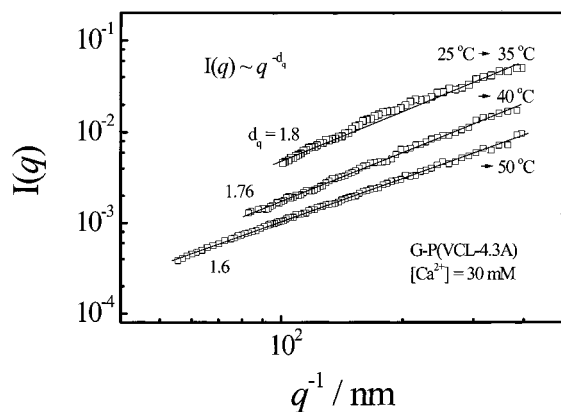


Figure 9. Double-logarithmic plots of scattering intensity $I(q)$ vs scattering vector q for resultant microgel aggregates formed at different aggregation temperatures.

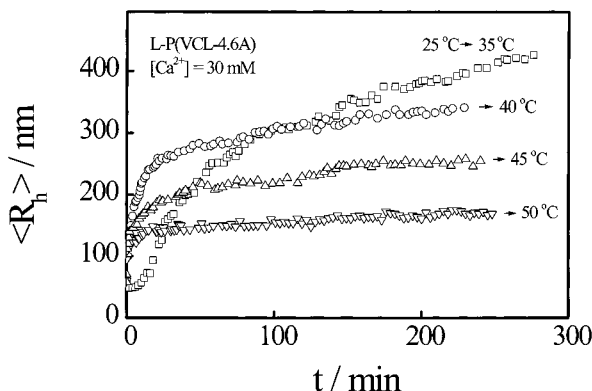


Figure 10. Time dependence of average hydrodynamic radius $\langle R_h \rangle$ of linear chain aggregates formed after the solution temperatures were suddenly increased to different aggregation temperatures.

together by Ca^{2+} . The higher the temperature, the faster the collapse. It is expected that in a fast shrinking process more COO^- groups are trapped inside, so that the number of effective COO^- groups on the periphery decreases. Therefore, the binding probability between two collided microgels reduces. Further, we should consider the surface curvature of collapsed microgels. For less collapsed microgels, the surface is relatively flat so that two microgels can be stuck together via more $\text{Ca}^{2+}(\text{COO}^-)_2$ complexation points, resulting in a stronger binding. For fully collapsed microgels, the surface curvature limits the number of the complexation between two microgels. Figure 9 shows that $I(q)$ is scaled to q as $I(q) \propto q^{-d_q}$ with d_q in the range 1.6–1.8. The slight decrease of d_q as the temperature increases reveals that the aggregates formed at higher temperatures are relatively more open and less uniform.

In comparison, Figure 10 shows the aggregation of linear chains at different temperatures. As in the case of microgels, the resultant aggregates become smaller when the temperature is higher. At 35 °C, there exists a short initial induction period in which there is no apparent interchain aggregation. Figure 11 shows a corresponding scaling between $I(q)$ and q for the resultant aggregates made of linear chains. d_q decreases as the aggregation temperatures increase. At 45 and 50 °C, d_q is similar to those observed in the aggregation of spherical microgels. Note that the complexation of linear chains could be either intrachain or interchain. The intrachain complexation leads to the chain contraction,

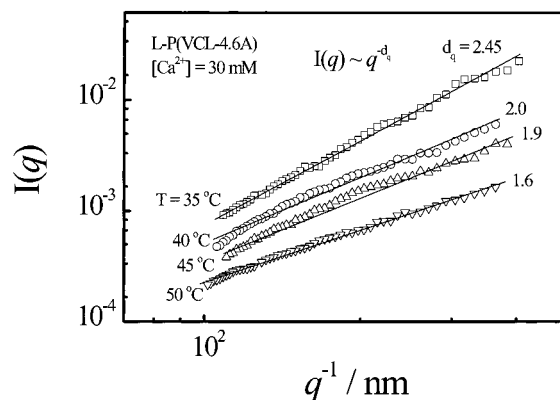


Figure 11. Double-logarithmic plots of scattering intensity $I(q)$ vs scattering vector q for resultant linear chain aggregates formed at different aggregation temperatures.

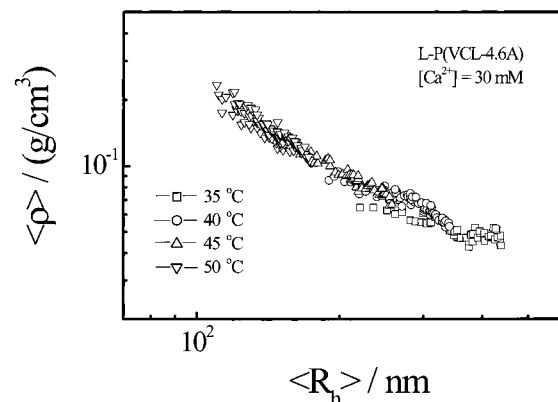


Figure 12. Double-logarithmic plots of aggregate size dependence of average chain density $\langle \rho \rangle$ vs average hydrodynamic radius $\langle R_h \rangle$ for resultant linear chain aggregates formed at different aggregation temperatures.

and only the interchain complexation results in the aggregation. The two processes always compete in a real experiment. At a lower aggregation temperature, individual crumpled chains are able to interpenetrate each other to form a more uniform structure. As the aggregation temperature increases, the collapse of individual chains becomes so fast that individual chains have less chance to undergo the interchain complexation in a dilute solution. Therefore, the complexation at higher temperatures mainly happens between highly collapsed small clusters, similar to the complexation between those collapsed microgels. Therefore, less interchain penetration occurs at higher temperatures, as illustrated in Figure 7.

Figure 12 reveals that, despite different values of d_q shown in Figure 11, the plots of $\langle \rho \rangle$ vs $\langle R_h \rangle$ for different temperatures collapse together. It is clear that in the initial stage small linear chain aggregates formed at 35 °C have a lower chain density. This is because linear chains were not fully collapsed at 35 °C, and the interpenetration of different chains at the initial stage was less. At higher temperatures, linear chains were more collapsed so that as the aggregation temperature increases, the chain density increases, but the size of the aggregates decreases, supporting the results in Figure 10, namely, a higher aggregation temperature leads to the aggregates with a more open and less uniform structure.

Figure 13 shows that, for the aggregation of microgels at 35 °C, the aggregation rate and the size and molar

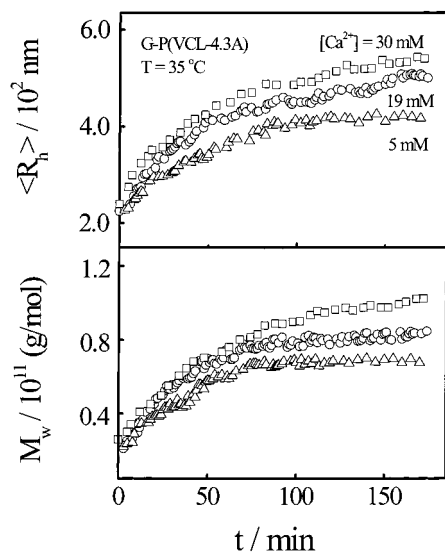


Figure 13. Temperature dependence of average hydrodynamic radius $\langle R_h \rangle$ and weight-average molar mass M_w of microgel aggregates formed in the presence of different amounts of Ca^{2+} .

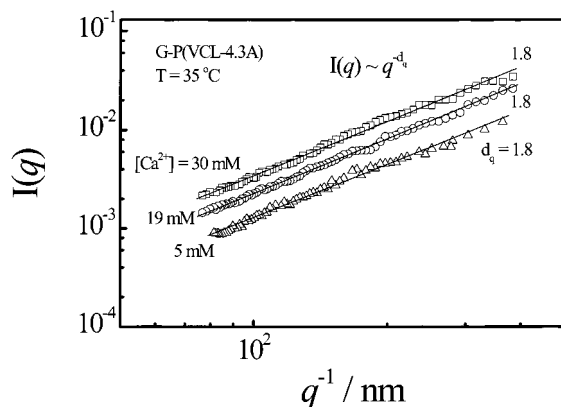


Figure 14. Double-logarithmic plots of scattering intensity $I(q)$ vs scattering vector q for resultant microgel aggregates formed in the presence of different amounts of Ca^{2+} .

mass of the resultant aggregates increase with the Ca^{2+} concentrations. This is because more Ca^{2+} ions can enhance the sticking probability of two collided microgels via the $\text{Ca}^{2+}/\text{COO}^-$ complexation. However, a similar scaling of $I(q)$ vs q shown in Figure 14 reveals that the structure of the resultant aggregates is independent of the Ca^{2+} concentration. The aggregation at 35°C leads to a structure with d_f in the range 1.7–1.9, which agrees well with the DLCA model. Figure 15 shows that the plots of M_w vs $\langle R_h \rangle$ in the presence of three different amounts of Ca^{2+} ions collapse into a single line of $M_w \propto \langle R_h \rangle^{d_f}$ with $d_f = 1.8 \pm 0.1$, further indicating that the Ca^{2+} concentration has no influence on the structure of the resultant aggregates. A combination of Figures 13–15 shows that, despite different aggregation rates and the aggregate sizes, the aggregation mechanism and the aggregate structure are not influenced by the cation concentration as long as the ratio of $[\text{Ca}^{2+}]/[\text{COO}^-]$ is much higher than the stoichiometric ratio (1:2).

In comparison, Figure 16 shows that for linear chains both the complexation rate and the aggregate size also increase with the Ca^{2+} concentration. Note that when $[\text{Ca}^{2+}] = 5 \text{ mM}$, there is no apparent interchain complexation even though the ratio of $[\text{Ca}^{2+}]/[\text{COO}^-]$ is

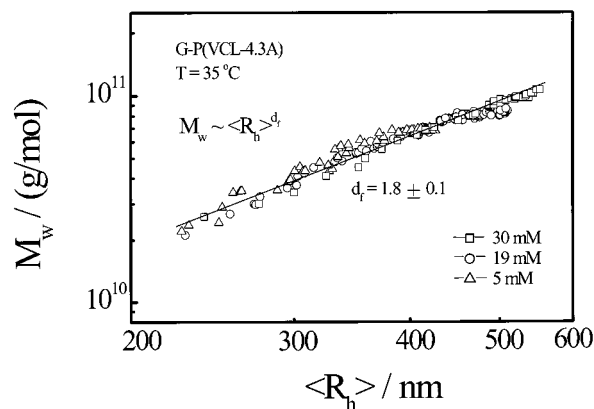


Figure 15. Double-logarithmic plots of weight-average molar mass M_w vs average hydrodynamic radius $\langle R_h \rangle$ of resultant microgel aggregates formed in the presence of different amounts of Ca^{2+} .

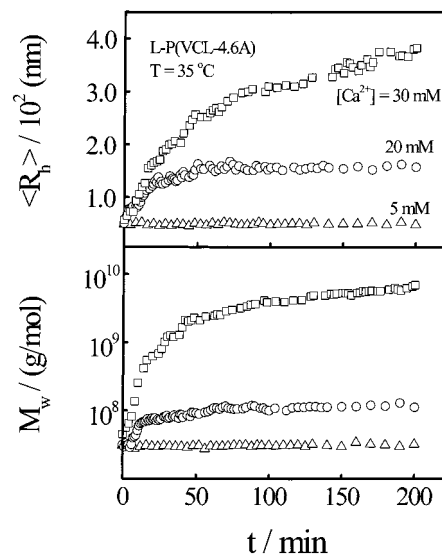


Figure 16. Time dependence of average hydrodynamic radius $\langle R_h \rangle$ and weight-average molar mass M_w for resultant linear chain aggregates formed in the presence of different amounts of Ca^{2+} .

already hundreds times higher than the stoichiometric one (1:2). In comparison with the aggregation of spherical microgels under the same conditions, the $\text{Ca}^{2+}/\text{COO}^-$ complexation induced aggregation of linear chains is less effective. Note that at 35°C each linear chain is not fully collapsed, and the COO^- groups are uniformly distributed in its hydrodynamic volume, while the shrinking of microgels forces more COO^- groups on surface. Therefore, it is much easier for two collided microgels to stick together. Figure 17 shows that the scaling of $I(q)$ to q is similar, revealing that the structure of the resultant aggregates is also not affected by the Ca^{2+} concentration. The higher fractal dimension d_f of the linear chain aggregates has been discussed before.

Conclusions

We have shown that the $\text{Ca}^{2+}/\text{COO}^-$ complexation induced aggregation of thermally sensitive poly(*N*-vinylcaprolactam-*co*-sodium acrylate) spherical microgels is essentially governed by the diffusion-limited cluster–cluster aggregation (DLCA) mechanism, leading to the aggregates with a fractal dimension d_f in the range 1.7–1.9. The chain density of the resultant aggregates increases with the sodium acrylate content.

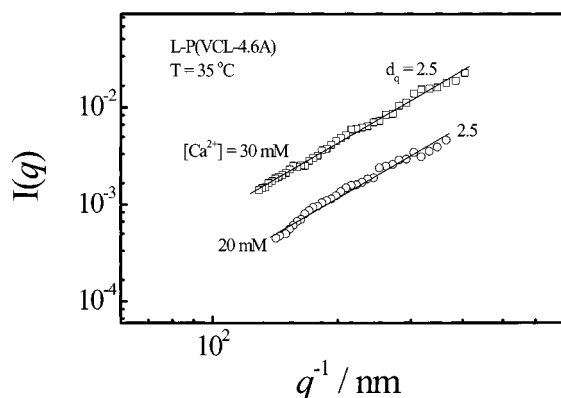


Figure 17. Double-logarithmic plots of scattering intensity $I(q)$ vs scattering vector q for resultant linear chain aggregates in the presence of different amounts of Ca^{2+} .

The increase of Ca^{2+} concentration can speed up the aggregation and result in larger aggregates but has no influence on the aggregation mechanism and the aggregate structure. We also found that the fractal dimension and the chain density of the resultant aggregates slightly decreased as the aggregation temperature increased. As for poly(*N*-vinylcaprolactam-co-sodium acrylate) linear chains, the situation is more complicated because the chain conformation varies with the aggregation temperature. We have revealed, for the first time, that the fractal dimension of linear chain aggregates was dependent on the initial chain conformation. At a relatively lower aggregation temperature, the contraction of individual chains was accompanied by an extensive interchain penetration and aggregation. The resultant aggregates are more uniform. As the aggregation temperature increases, the collapse of individual chains is much faster they have less chance to undergo the interchain aggregation. Therefore, the $\text{Ca}^{2+}/\text{COO}^-$ complexation mainly happens between highly collapsed small clusters, resulting in a more open and less uniform structure, similar to that formed in the aggregation of spherical microgels. The fractal dimension of the resultant linear chain aggregates decreases from 2.5 to 1.6 as the aggregation temperature increases from 35 to 50 °C.

Acknowledgment. The financial support of the Special Funds for Major State Basic Research Projectors (G1999064800), the CAS Bai Ren Project, the NNSFC projector (29974027), and the HKSAR Earmarked RGC Grants (CUHK 4266/00P, 2160135) is gratefully acknowledged.

References and Notes

- (1) Magazu, S.; Maisano, G.; Mallamace, F.; Micali, N. *Phys. Rev. A* **1989**, *39*, 4195.
- (2) Meakin, P. *Phys. Rev. Lett.* **1983**, *51*, 1119.
- (3) Martin, J. E.; Ackerson, B. J. *Phys. Rev. A* **1985**, *31*, 1180.
- (4) Jullien, R.; Botet, R.; Mors, P. M. *Faraday Discuss. Chem. Soc.* **1987**, *83*, 125.
- (5) Reinecke, H.; Fazel, N.; Dosiere, M.; Guenet, J. M. *Macromolecules* **1997**, *30*, 8360.
- (6) Aubert, C.; Cannell, D. S. *Phys. Rev. Lett.* **1986**, *56*, 738.
- (7) Tang, P.; Colflesh, D. E.; Chu, B. J. *Colloid Interface Sci.* **1988**, *126*, 304.
- (8) Lin, M. Y.; Lindsay, H. M.; Weitz, D. A.; Ball, R. C.; Klein, R.; Meakin, P. *Nature* **1989**, *40*, 4665.
- (9) Micali, N.; Mallamace, F.; Romeo, A.; Purrello, R.; Scolaro, L. *J. Phys. Chem. B* **2000**, *104*, 5897.
- (10) Botet, R.; Kolb, M.; Jullien, R. In *Physics of Finely Divided Matter*; Boccara, N., Daoud, M., Eds.; Springer-Verlag: New York, 1985.
- (11) Zhou, Z.; Chu, B. J. *Colloid Interface Sci.* **1991**, *143*, 356.
- (12) Mandlbrot, B. J. *Fractals, Form and Dimensions*; Freeman: San Francisco, 1977.
- (13) Weitz, D. A.; Huang, J. S.; Lin, M. Y.; Sung, J. *Phys. Rev. Lett.* **1985**, *54*, 1416.
- (14) Peng, S.; Wu, C. *Macromolecules* **1999**, *32*, 585.
- (15) Brown, W. D.; Ball, R. C. *J. Phys. A* **1985**, *18*, L 517.
- (16) Vicsek, T. *Fractal Growth Phenomena*; World Scientific: London, 1992.
- (17) Halsey, T. C. *Phys. Today* **2000**, *11*, 36.
- (18) Aymard, P.; Nicolai, T.; Durand, D.; Clark, A. *Macromolecules* **1999**, *32*, 2542.
- (19) Kim, A. Y.; Berg, J. C. *Langmuir* **2000**, *16*, 2101.
- (20) Takata, S.; Norisuye, T.; Tanaka, N.; Shibayama, M. *Macromolecules* **2000**, *33*, 5470.
- (21) Pelletier, O.; Davidson, P.; Bourgaux, C.; Coulon, C.; Regnault, S.; Livage, J. *Langmuir* **2000**, *16*, 5295.
- (22) Mitsuo, N.; Tomohide, N.; Yoshiki, N.; Syogo, W. *J. Chem. Phys.* **1999**, *110*, 2711.
- (23) Kabanov, V. *Makromol. Chem., Macromol. Symp.* **1991**, *48/49*, 425.
- (24) Tsuchida, E.; Abe, K. *Adv. Polym. Sci.* **1982**, *45*, 1130.
- (25) Pogodina, N. V.; Tsvetkov, N. V. *Macromolecules* **1997**, *30*, 4897.
- (26) Dai, S.; Tam, K. C.; Jenkins, R. D. *Macromolecules* **2000**, *33*, 404.
- (27) Kjoniksen, A.; Joabsson, F.; Thuresson, K.; Nystroem, B. *J. Phys. Chem. B* **1999**, *103*, 9818.
- (28) Bakeev, K. N.; Isumrudov, V. A.; Kuchanov, S. I.; Zezin, A. B.; Kabanov, V. A. *Macromolecules* **1992**, *25*, 4249.
- (29) Tsianou, M.; Kjoniksen, A.; Thuresson, K.; Nystrom, B. *Macromolecules* **1999**, *32*, 2974.
- (30) Vishalakshi, B.; Ghosh, S.; Kalpagam, V. *Polymer* **1993**, *34*, 3270.
- (31) Lau, C. W.; Wu, C. *Macromolecules* **1999**, *32*, 581.
- (32) Wu, C.; Xia, K. Q. *Rev. Sci. Instrum.* **1994**, *65*, 587.
- (33) Berne, B. J.; Pecora, R. *Dynamic Light Scattering*; Plenum Press: New York, 1976.
- (34) Chu, B. *Laser Light Scattering*, 2nd ed.; Academic Press: New York, 1991.
- (35) Stockmayer, W. H.; Schimidt, M. *Pure Appl. Chem.* **1982**, *54*, 407.

MA010376C